Letter

Hybrid *s*-wave superconductivity in CrB_2

Sananda Biswas,[1,*] Andreas Kreisel,[2,3,†] Adrian Valadkhani,[1] Matteo Dürrnagel,[4,5] Tilman Schwemmer,[4] Ronny Thomale,[4] Roser Valentí,[1] and Igor I. Mazin[6,7]

[1]*Institut für Theoretische Physik, Goethe-Universität Frankfurt, 60438 Frankfurt am Main, Germany*
[2]*Institut für Theoretische Physik, Universität Leipzig, Brüderstraße 16, 04103 Leipzig, Germany*
[3]*Niels Bohr Institute, University of Copenhagen, 2100 Copenhagen, Denmark*
[4]*Julius-Maximilians-Universität Würzburg, 97070 Würzburg, Germany*
[5]*Institute for Theoretical Physics, ETH Zürich, 8093 Zürich, Switzerland*
[6]*Department of Physics and Astronomy, George Mason University, Fairfax, Virginia 22030, USA*
[7]*Quantum Science and Engineering Center, George Mason University, Fairfax, Virginia 22030, USA*

(Received 8 November 2022; revised 12 June 2023; accepted 13 June 2023; published 5 July 2023)

In a metal with multiple Fermi pockets, the formation of *s*-wave superconductivity can be conventional due to electron-phonon coupling or unconventional due to spin fluctuations. We analyze the hexagonal diboride CrB_2, which is an itinerant antiferromagnet at ambient conditions and turns superconducting upon increasing pressure. While the high-pressure behavior of T_c suggests conventional *s*-wave pairing, we find that spin fluctuations promoting unconventional *s*-wave pairing become important in the vicinity of the antiferromagnetic dome. As the symmetry class of the *s*-wave state is independent of its underlying mechanism, we argue that CrB_2 is a realization of a *hybrid s*-wave superconductor where unconventional and conventional *s*-wave mechanisms team up to form a joint superconducting dome.

DOI: 10.1103/PhysRevB.108.L020501

Introduction. Even though the phenomenological description of a superconducting state finds its common ground in the notion of a phase-coherent superposition of Cooper pairs and the mean-field description derived thereof [1], the possible microscopic formation mechanism is highly diverse. In a so-called conventional superconductor (CS), electron-phonon coupling generates an effective attractive electron-electron interaction [2–4]. Not only do phonons promote zero-angular-momentum Cooper pairs, i.e., an *s*-wave type pairing function, but the electron-phonon interaction also tends to be relatively momentum independent, a few exceptions not withstanding, and gives rise to a reasonably uniform gap, $\Delta_{\mathrm{CS}}(\mathbf{k}) \sim \text{const}$, throughout the Brillouin zone.

For unconventional superconductivity (UCS), which has most prominently surfaced in the context of the high-T_c cuprates, the microscopic footing of pairing appears both more diverse and less understood. From the viewpoint of spin fluctuations [5], electron pairing can originate from repulsive electron-electron interactions [6,7]. However, this implies that the gap function is sign changing in the Brillouin zone, leading to the condition $(\langle\Delta_{\mathrm{UCS}}(\mathbf{k})\rangle^2_{\mathrm{BZ}} \ll \langle\Delta^2_{\mathrm{UCS}}(\mathbf{k})\rangle_{\mathrm{BZ}})$. For a single-pocket Fermi surface, this naturally suggests the presence of nodes and thus a principal unconventional superconducting gap that is qualitatively different from the conventional one. For multiple Fermi pockets, however, nodes are avoidable for unconventional pairing by allowing sign changes of Δ between the pockets. This is at the heart of the nature of superconducting pairing in iron pnictide superconductors [8,9], where the compensated metal parent state forms superconducting pairing of opposite sign for hole and electron pockets, respectively. For each individual pocket, the gap may appear rather uniform, even though typically not as uniform as for a conventional superconducting state. Note that from the viewpoint of symmetry, such an unconventional superconducting gap cannot be distinguished from a conventional *s* wave: in both cases, the zero-momentum Cooper pair is described by the irreducible point-group representation with trivial characters. Yet, even though the *angular* dependence of the superconducting gap as a function of the wave vector is the same, the *radial* part shifts away from approximately constant in the conventional superconductor, referred to as s_{++}, to exhibit strong k dependence in the unconventional case, which is referred to as s_{+-}.

Since an *s*-wave superconductor can exist both as a conventional s_{++} and as an unconventional s_{+-}, in principle, a *hybrid s-wave superconductor* can be imagined, where unconventional and conventional pairing mechanisms team up to yield one continuous *s*-wave superconducting region spanning both CS and UCS domains. This intriguing possibility, however, requires a hypothetical material where spin fluctuations and phonons have a possibility to cooperate at least to some extent. More specifically, the latter have to peak at small wave vector, while the former (as long as we are not considering triplet pairing) necessarily have to have a maximum at a particular wave vector matching the Fermi surface geometry.

While iron pnictide superconductors seem to be a promising host for a hybrid superconducting state, the conventional and unconventional pairing are too imbalanced because of good Fermi-surface nesting enhancing the spin-fluctuation (SF) mechanism, as compared to weak electron-phonon

*biswas@itp.uni-frankfurt.de
†kreisel@nbi.ku.dk

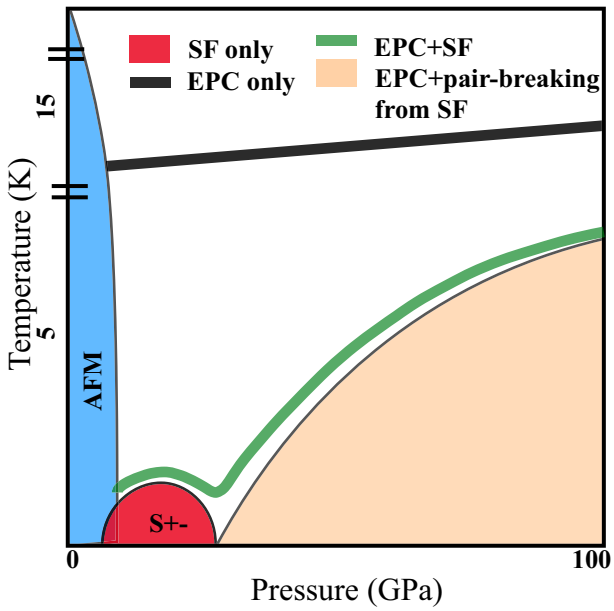

FIG. 1. Proposed schematic temperature-pressure phase diagram for a hybrid s-wave superconductor. Spin fluctuation limit: Antiferromagnetic region with maximum T_{AFM} at ambient pressure (blue region), dropping rapidly with pressure and followed by (possibly overlapping with) a smaller unconventional superconducting dome near the quantum critical point (red region). Electron-phonon limit: T_c is only weakly dependent on pressure and dominates the high-pressure part of the phase diagram (light-orange region). The hybrid s wave (green) appears in the crossover region between the two limits where the pair-breaking impact of spin fluctuations is vital for explaining the drop of T_c towards ambient pressure.

coupling (EPC) [10]. In addition, EPC does not satisfy the requirement to peak at small q (i.e., in the intraband channel) either. In fact, the competition between SF and EPC has been under scrutiny for quite a few superconducting materials [11–15], but no suitable candidate has been identified so far, exhibiting not only competition, but also collaboration between the two mechanisms in some range of parameters.

In this Letter, we propose CrB_2 as a potential hybrid s-wave superconductor, continuously tunable by pressure between the s_{+-} and s_{++} limits. Indeed, superconductivity has recently been discovered in CrB_2 under pressure, with a maximum T_c of 7 K [16]. Isostructural to the conventional superconductor MgB_2 [17,18], CrB_2 exhibits itinerant antiferromagnetism at ambient pressure. T_c is found to weakly increase with pressure at odds with the typical dome formation in unconventional superconductors. This is a strong indication that at least beyond a certain pressure regime, superconducting pairing in CrB_2 is dominated by the electron-phonon coupling. Due to the proximity to the antiferromagnetic order, however, the superconductivity in CrB_2 is likely to be of unconventional nature at lower pressure, since spin fluctuations are crucial near a magnetic quantum critical point. From our synoptic analysis of superconductivity, accounting for both electron-phonon coupling and spin fluctuations, we find that CrB_2 is a likely candidate for a hybrid s-wave superconductor, as summarized in Fig. 1. On the one hand, spin fluctuations promoting s_{+-} type are highly relevant due to significant nesting of the CrB_2 Fermi surface (note that here the three-dimensional nesting is present due to the flat parts in the Fermi surface in the k_x-k_y plane with large density of states). On the other hand, our calculations yield rather strong electron-phonon coupling, with the main contribution coming from around the Brillouin-zone center, Γ, enabling a significant cooperative effect between the two mechanisms. The interplay of both pairing tendencies culminates in the schematic temperature-pressure phase diagram depicted in Fig. 1 (green line): The superconducting domain in the high-pressure limit is dominated by the electron-phonon mechanism, which, if let alone, would suggest a fairly constant T_c throughout the phase diagram (black line) with no indication for competitive orders. By contrast, only spin fluctuations related to the antiferromagnetic order at the ambient pressure would generate unconventional superconductivity within a small pressure range and a significantly lower T_c than T_{AFM} (red dome). Taken together, however, electron-phonon couplings and spin fluctuations suggest a crossover between the two limiting scenarios, where, starting from the center of the superconducting region, spin fluctuations act upon the s-wave superconductor as pair breakers close to the antiferromagnetic phase at lower pressure and the electron-phonon coupling determines the scale of saturating superconducting pairing for higher pressure.

Methods. First, we investigate the superconducting pairing from a pure electron-electron interaction perspective adapting the spin-fluctuation pairing mechanism expected to be present for the correlated Cr $3d$ orbitals. To this end, we set up the pairing interaction in the random-phase approximation (RPA) [19,20] and solve the linearized gap equation for a discretization of the three-dimensional Fermi surface [21–23], yielding the eigenvalues, λ_i, and the gap eigenfunctions, $g_i(\mathbf{k})$, proportional to the superconducting order parameter. Next, we examine the electron-phonon mechanism by calculating the pressure dependence of the phonon dispersion, electron-phonon linewidth, γ, and electron-phonon coupling constants, λ, using density functional perturbation theory as implemented in the QUANTUM ESPRESSO code [24].

Results. CrB_2 crystallizes in a $P6/mmm$ structure (space group 191) with $c/a > 1$ at ambient pressure. As a function of pressure the c parameter decreases more rapidly than a, and around 30 GPa the ratio c/a becomes less than 1 with no observed changes in the crystal structure [16]. While the Mg states in MgB_2 lie far away from the Fermi surface, the band structure of CrB_2 suggests significant contributions from Cr $3d$ orbitals near the Fermi surface at all pressures (see Fig. 2 for the 100 GPa case), along with contributions coming from B atoms [23]. This makes the properties of CrB_2 markedly different from the isostructural MgB_2 [25], as we will discuss below. Accounting for the spin-density-wave instability at low pressures [16,26], we tune the bare Coulomb interaction responsible for the spin fluctuations such that the RPA instability occurs roughly at $p_c = 16$ GPa and then calculate pairing eigenvalues λ_i as a function of pressure. Figure 3 reveals the two main results from this investigation: First, the eigenvalues λ_i and therefore also the pairing strength rapidly decrease as a function of pressure, making this pairing interaction practically irrelevant at large pressures. Second, the leading instability is clearly of sign-changing s_{+-} type over a large pressure range with one exception very close to

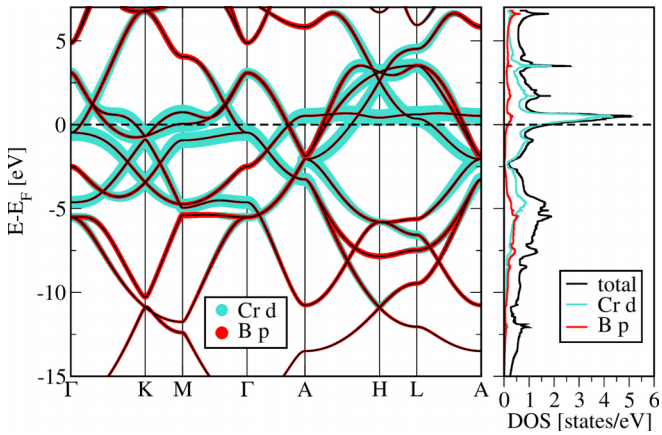

FIG. 2. Electronic band structure and density of states (DOS) at 100 GPa. Fat bands and DOS of Cr $3d$ states (cyan) and B $2p$ states (red) show that both states contribute to the formation of the Fermi surface.

p_c. The order parameter has one sign at a band forming a flat part at finite k_z close to the Brillouin zone boundary and opposite sign at the Fermi surface appearing around the Γ point (see Supplemental Material [23] for top views). Higher order s-wave solutions or solutions with higher angular momentum are subleading and their eigenvalues exhibit peaks from Van Hove singularities moving through the Fermi level close to 72 and 86 GPa. The eigenvalues show weak dependence on the temperature at which the pairing interaction is evaluated [23].

In order to examine the electron-phonon pairing and the expected critical temperature from a material-specific perspective, we first determine the strength of the electron-phonon

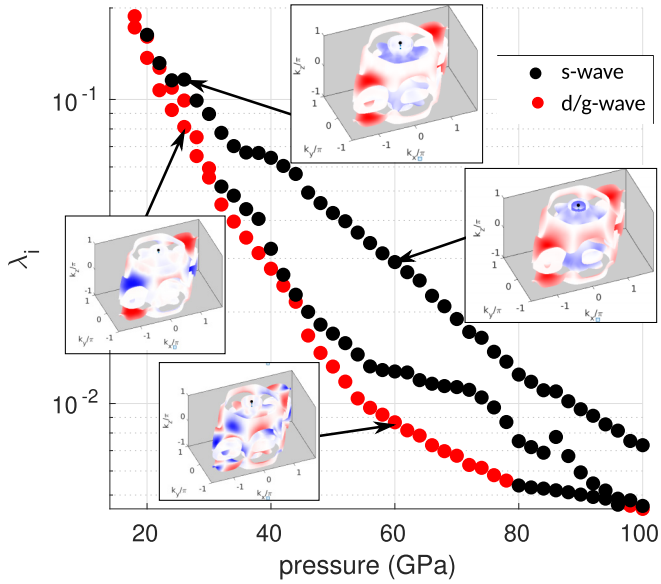

FIG. 3. Spin-fluctuation pairing. Eigenvalues λ_i of the leading and subleading instabilities as a function of pressure as calculated with $U = 0.124$ eV where the critical pressure is $p_c = 16$ GPa. All calculations are at fixed temperature $T = 0.02$ eV. Insets: Gap function $g_i(\mathbf{k})$ on the Fermi surface of the leading s-wave (black circles) state and d/g-wave (red circles) state for two representative pressures of 26 and 60 GPa as indicated by the arrows. Red and blue regions represent two opposite signs of the gap function.

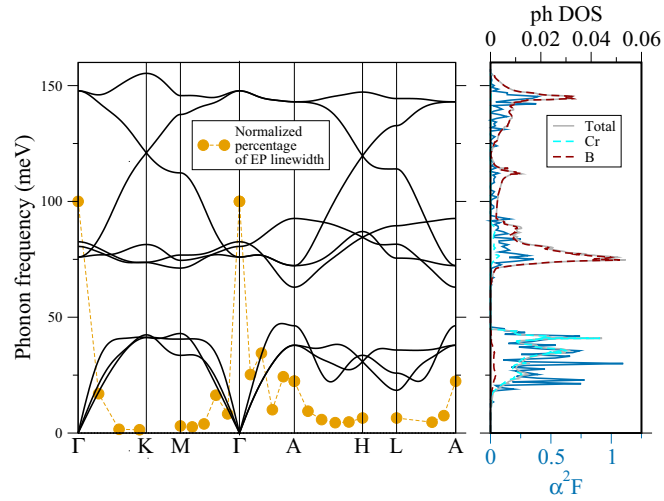

FIG. 4. Phonon dispersion, electron-phonon (EP) linewidth, spectral function $[\alpha^2F(\omega)]$, and phonon density of states (ph DOS) of the relaxed structure at 100 GPa. Normalized percentage of EP linewidth (orange) is equal to $\gamma/\gamma_{\max} \times 100\%$ and is strongly peaked at zone center, Γ.

coupling constant, λ. Experimentally, the system is reported to have the largest T_c around 100 GPa; therefore, we first focus on this pressure region. The relaxed structure at 100 GPa has a ratio $c/a = 0.93$ [whereas $(c/a)_{\text{exp}} = 0.96$] with all phonon modes being stable. We therefore have chosen this structure for establishing convergence criteria for λ with respect to **k** mesh, **q** mesh, and Gaussian broadening (see Ref. [23]). The converged value of $\lambda = 0.78$ has significant contributions to the electron-phonon spectral function, $\alpha^2F(\omega)$, from the low-frequency vibrations involving Cr atoms as seen in Fig. 4. Note that the phonon dispersions calculated with the experimental structure [16] exhibit an imaginary acoustic mode along the **k** path perpendicular to the honeycomb boron plane. Though this indicates an instability toward a charge density wave state, zero-point vibrational effects can stabilize the conventional structure [23]. Nonetheless, an estimate of the lower bound for $\lambda = 0.60$ could be obtained by excluding the imaginary acoustic mode at 100 GPa.

The electron-phonon linewidth, γ (plotted as $\gamma/\gamma_{\max} \times 100\%$), exhibits maximum contribution around the Brillouin-zone center, i.e., $\mathbf{q} = 0$, which suggests significantly stronger intraband electron-phonon coupling compared to interband contribution, giving rise to conventional s_{++} pairing. With the average phonon frequency softening at lower pressures, T_c is also reduced as pressure goes down. Our computed values of T_c, 14.3 K at 100 GPa and 13.6 K at 60.7 GPa, support this interpretation and justifies our sketch of the electron-phonon driven contribution to T_c in Fig. 1.

Discussions. We have so far investigated the two pairing mechanisms individually, finding that the attractive electron-phonon pairing interaction is dominated by contributions close to $\mathbf{q} = 0$, thus exhibiting a large and positive intraband attractive interaction $V_{\text{intra}}^{\text{EPC}} > 0$, while the interband interaction is much smaller, $V_{\text{inter}}^{\text{EPC}} \ll V_{\text{intra}}^{\text{EPC}}$, leading to critical temperatures of $T_c = 7$ K. The pairing interaction from SF is generically repulsive (negative), but more repulsive for large

momentum transfer so that the interband pairing $V^{\mathrm{SF}}_{\mathrm{inter}} < 0$ is dominating over the intraband pairing $|V^{\mathrm{SF}}_{\mathrm{inter}}| \gg |V^{\mathrm{SF}}_{\mathrm{intra}}|$.

Close to the spin-density-wave instability, the spin fluctuations are enhanced, leading to a sizable pairing interaction, which then quickly decreases with pressure beyond the critical pressure p_c (pressure at which spin fluctuations diverge). Assuming the usual RPA mechanism, one can trace this back to the increase of the electronic bandwidth as a function of pressure, $W(p) \approx W_{\mathrm{AFM}}[1 + x(p - p_c)]$, where W_{AFM} is the bandwidth at the critical pressure p_c and the dependence is assumed to be expanded to first order close to p_c. Taking this into account, we obtain $V^{\mathrm{SF}}_{\mathrm{intra/inter}} \propto [\alpha_{\mathrm{intra/inter}} + x(p - p_c)]^{-1}$, where $\alpha_{\mathrm{intra/inter}}$ describes the closeness of the intra- (inter-) band scattering vectors to a nesting vector giving rise to a peak in the susceptibility [23].

Adding up the electron-phonon and the spin-fluctuation pairing interactions, one then arrives at the qualitative behavior of the critical temperature depicted in Fig. 1, where the spin fluctuations dominate close to p_c and a sign-changing order parameter emerges as the dominant instability. At larger pressures, the critical temperature is expected to decrease until the s_{+-} and s_{++} instabilities have comparable eigenvalues and the critical temperature increases again, since now the pair-breaking contribution from the spin fluctuations $V^{\mathrm{SF}}_{\mathrm{intra}}$ decreases as well and the sum $V^{\mathrm{EPC}}_{\mathrm{intra}} + V^{\mathrm{SF}}_{\mathrm{intra}}$ is dominated by the electron-phonon contribution. Note that despite the small eigenvalues for the SF pairing instability, the electronic contribution to pairing remains finite due to the momentum-independent Hubbard-Hund interaction, and pair breaking will remain non-negligible even at large pressures, where the expected T_c for the "SF alone" pairing is exponentially small. Effective T_c (green line in Fig. 1) thus gets reduced from the T_c computed from EPC only (black line).

Even though isostructural, CrB_2 therefore differs from the prototypical electron-phonon superconductor MgB_2, due to the following aspects: First, due to the presence of Cr $3d$ states, additional effects from these correlated states contribute to the fermiology of the system whereas Mg states in MgB_2 do not take part in the formation of Cooper pairs. Second, the isotropic electron-phonon coupling constants are comparable ($\lambda|_{\mathrm{CrB_2(100\ GPa)}} = 0.78$ and $\lambda|_{\mathrm{MgB_2(P=0\ GPa)}} = 0.71$); nonetheless, unlike MgB_2, the low-frequency Cr-phonon modes have significant contributions to the EP-spectral function.

Conclusions. In summary, we have presented a hybrid perspective of electron-phonon and spin-fluctuation pairing in order to explain the overall phase diagram of CrB_2 where T_c is found to increase at pressures far away from the antiferromagnetic instability, a behavior not expected for superconductors driven by spin fluctuations alone. Instead, the cooperative and anticooperative effects of the two pairing mechanisms allowed by the presence of a leading instability of the same symmetry explains the larger critical temperature at high pressure (far away from the antiferromagnetic order). Furthermore, the pairing state, while lowering pressure, is predicted to have a crossover from s_{++} to s_{+-} on approaching the quantum critical point with a nonmonotonous behavior of T_c. We have discussed in detail the differences between the well studied MgB_2 and the CrB_2 system; the latter has correlated d states close to the Fermi level and a dominating electron-phonon interaction at small momentum transfer; both of them are required ingredients for the appearance of the hybrid s-wave superconductivity which is expected to exhibit an anisotropic order parameter due to unconventional pairing. An experimental confirmation of the feasibility of this proposal would be a detailed spectroscopic investigation of spin fluctuations and their extension away from the critical point; the available resistivity data [16] so far reveals the antiferromagnetic dome but is unable to pinpoint the presence of fluctuations at higher pressures. Experimental signatures of the proposed scenario would be the nonmonotonous behavior of T_c close to the quantum critical point and the crossover to non-sign-changing order parameter with increasing pressure. The latter could be tested experimentally by observing the effect of disorder. At lower pressures the potential scatterers should lead to a strong suppression of T_c, while the s_{++} state at higher pressures should be almost unaffected according to Anderson's theorem. In fact, the resistivity measurement in Ref. [16] seems to indicate a Fermi-liquid to non-Fermi-liquid crossover at low temperature. The ability to not only tune T_c [27], but also the nature of the superconducting order parameter may open new perspectives in the study of unconventional superconductivity.

Acknowledgments. We thank Young-Joon Song, Paul Wunderlich, and Shinibali Bhattacharyya for discussions. S.B., A.V., and R.V. thank the Deutsche Forschungsgemeinschaft (DFG, German Research Foundation) through TRR 288-422213477 (Projects A05 and B05). A.K. acknowledges support by the Danish National Committee for Research Infrastructure (NUFI) through the ESS-Lighthouse Q-MAT. R.T. and R.V. acknowledge support from the DFG through QUAST FOR 5249-449872909 (Projects P3 and P4). I.I.M. acknowledges support from the U.S. Department of Energy through Grant No. DE-SC0021089 and from the Wilhelm and Else Heraeus Foundation. M.D., T.S., and R.T. acknowledge funding by the DFG through Project-ID 258499086–SFB 1170 and through the Würzburg-Dresden Cluster of Excellence on Complexity and Topology in Quantum Matter–ct.qmat Project ID 390858490–EXC 2147.

[1] J. Bardeen, L. N. Cooper, and J. R. Schrieffer, Theory of superconductivity, Phys. Rev. **108**, 1175 (1957).

[2] G. M. Eliashberg, Zh. Eksp. Teor. Fiz. **38**, 966 (1960) [Sov. Phys. JETP **11**, 696 (1960)].

[3] Y. Nambu, Quasi-particles and gauge invariance in the theory of superconductivity, Phys. Rev. **117**, 648 (1960).

[4] P. Morel and P. W. Anderson, Calculation of the superconducting state parameters with retarded electron-phonon interaction, Phys. Rev. **125**, 1263 (1962).

[5] W. Kohn and J. M. Luttinger, New Mechanism for Superconductivity, Phys. Rev. Lett. **15**, 524 (1965).

[6] C. Gros, R. Joynt, and T. Rice, Superconducting instability in the large-U limit of the two-dimensional Hubbard model, Z. Phys. B **68**, 425 (1987).

[7] S. R. White, D. J. Scalapino, R. L. Sugar, N. E. Bickers, and R. T. Scalettar, Attractive and repulsive pairing interaction vertices for the two-dimensional Hubbard model, Phys. Rev. B **39**, 839 (1989).

[8] I. I. Mazin, D. J. Singh, M. D. Johannes, and M. H. Du, Unconventional Superconductivity with a Sign Reversal in the Order Parameter of $LaFeAsO_{1-x}F_x$, Phys. Rev. Lett. **101**, 057003 (2008).

[9] P. Hirschfeld, M. Korshunov, and I. Mazin, Gap symmetry and structure of Fe-based superconductors, Rep. Prog. Phys. **74**, 124508 (2011).

[10] L. Boeri, O. V. Dolgov, and A. A. Golubov, Is $LaFeAsO_{1-x}F_x$ an Electron-Phonon Superconductor? Phys. Rev. Lett. **101**, 026403 (2008).

[11] T. S. Nunner, J. Schmalian, and K. H. Bennemann, Influence of electron-phonon interaction on spin-fluctuation-induced superconductivity, Phys. Rev. B **59**, 8859 (1999).

[12] L. Ortenzi, S. Biermann, O. K. Andersen, I. I. Mazin, and L. Boeri, Competition between electron-phonon coupling and spin fluctuations in superconducting hole-doped CuBiSo, Phys. Rev. B **83**, 100505(R) (2011).

[13] O. V. Dolgov, I. I. Mazin, A. A. Golubov, S. Y. Savrasov, and E. G. Maksimov, Critical Temperature and Enhanced Isotope Effect in the Presence of Paramagnons in Phonon-Mediated Superconductors, Phys. Rev. Lett. **95**, 257003 (2005).

[14] N. Witt, J. M. Pizarro, J. Berges, T. Nomoto, R. Arita, and T. O. Wehling, Doping fingerprints of spin and lattice fluctuations in moiré superlattice systems, Phys. Rev. B **105**, L241109 (2022).

[15] I. Schnell, I. I. Mazin, and A. Y. Liu, Unconventional superconducting pairing symmetry induced by phonons, Phys. Rev. B **74**, 184503 (2006).

[16] C. Pei, P. Yang, C. Gong, Q. Wang, Y. Zhao, L. Gao, K. Chen, Q. Yin, S. Tian, C. Li *et al.*, Pressure-induced superconductivity in itinerant antiferromagnet CrB_2, arXiv:2109.15213.

[17] J. Nagamatsu, N. Nakagawa, T. Muranaka, Y. Zenitani, and J. Akimitsu, Superconductivity at 39 K in magnesium diboride, Nature (London) **410**, 63 (2001).

[18] I. Mazin and V. Antropov, Electronic structure, electron-phonon coupling, and multiband effects in MgB_2, Phys. C (Amsterdam, Neth.) **385**, 49 (2003).

[19] S. Graser, T. A. Maier, P. J. Hirschfeld, and D. J. Scalapino, Near-degeneracy of several pairing channels in multiorbital models for the Fe pnictides, New J. Phys. **11**, 025016 (2009).

[20] M. Altmeyer, D. Guterding, P. J. Hirschfeld, T. A. Maier, R. Valentí, and D. J. Scalapino, Role of vertex corrections in the matrix formulation of the random phase approximation for the multiorbital Hubbard model, Phys. Rev. B **94**, 214515 (2016).

[21] A. Kreisel, Y. Wang, T. A. Maier, P. J. Hirschfeld, and D. J. Scalapino, Spin fluctuations and superconductivity in $K_xFe_{2-y}Se_2$, Phys. Rev. B **88**, 094522 (2013).

[22] M. Dürrnagel, J. Beyer, R. Thomale, and T. Schwemmer, Unconventional superconductivity from weak coupling, Eur. Phys. J. B **95**, 112 (2022).

[23] See Supplemental Material at http://link.aps.org/supplemental/10.1103/PhysRevB.108.L020501 for hybrid s-wave superconductivity in CrB_2 which gives details of the EPC and SF calculations and contains Refs. [16,19,21,22,24,28–34].

[24] P. Giannozzi, S. Baroni, N. Bonini, M. Calandra, R. Car, C. Cavazzoni, D. Ceresoli, G. L. Chiarotti, M. Cococcioni, and I. Dabo, QUANTUM ESPRESSO: A modular and open-source software project for quantum simulations of materials, J. Phys.: Condens. Matter **21**, 395502 (2009).

[25] J. Kortus, I. I. Mazin, K. D. Belashchenko, V. P. Antropov, and L. L. Boyer, Superconductivity of Metallic Boron in MgB_2, Phys. Rev. Lett. **86**, 4656 (2001).

[26] A. Bauer, A. Regnat, C. G. F. Blum, S. Gottlieb-Schönmeyer, B. Pedersen, M. Meven, S. Wurmehl, J. Kuneš, and C. Pfleiderer, Low-temperature properties of single-crystal CrB_2, Phys. Rev. B **90**, 064414 (2014).

[27] D. N. Basov and A. V. Chubukov, Manifesto for a higher T_c, Nat. Phys. **7**, 272 (2011).

[28] K. Koepernik and H. Eschrig, Full-potential nonorthogonal local-orbital minimum-basis band-structure scheme, Phys. Rev. B **59**, 1743 (1999).

[29] J. P. Perdew and Y. Wang, Accurate and simple analytic representation of the electron-gas correlation energy, Phys. Rev. B **45**, 13244 (1992).

[30] G. Kresse and J. Hafner, *Ab initio* molecular dynamics for liquid metals, Phys. Rev. B **47**, 558 (1993).

[31] S. Baroni, S. de Gironcoli, A. Dal Corso, and P. Giannozzi, Phonons and related crystal properties from density-functional perturbation theory, Rev. Mod. Phys. **73**, 515 (2001).

[32] W. L. McMillan, Transition temperature of strong-coupled superconductors, Phys. Rev. **167**, 331 (1968).

[33] P. B. Allen and R. C. Dynes, Transition temperature of strong-coupled superconductors reanalyzed, Phys. Rev. B **12**, 905 (1975).

[34] J. Beyer, J. B. Hauck, and L. Klebl, Reference results for the momentum space functional renormalization group, Eur. Phys. J. B **95**, 65 (2022).

Supplemental Material: Hybrid s-wave superconductivity in CrB_2

Sananda Biswas,[1,*] Andreas Kreisel,[2,3,†] Adrian Valadkhani,[1] Matteo Dürrnagel,[4] Tilman Schwemmer,[4] Ronny Thomale,[4] Roser Valentí,[1] and Igor I. Mazin[5,6]

[1] *Institut für Theoretische Physik, Goethe-Universität Frankfurt, 60438 Frankfurt am Main, Germany*
[2] *Institut für Theoretische Physik, Universität Leipzig, Brüderstr. 16, 04103 Leipzig, Germany*
[3] *Niels Bohr Institute, University of Copenhagen, 2100 Copenhagen, Denmark*
[4] *Julius-Maximilians-Universität Würzburg, Würzburg, Germany*
[5] *Department of Physics and Astronomy, George Mason University, Fairfax, VA 22030*
[6] *Quantum Science and Engineering Center, George Mason University, Fairfax, VA 22030*

(Dated: June 12, 2023)

This Supplementary Material contains details on the calculations for the spin-fluctuation pairing and electron phonon paring and discusses the charge density wave states. We include a section on a simplified two band model capable to capture the hybrid pairing properties as spin-fluctuations and electron phonon pairing gets modified by pressure and discuss feasibility of a functional renormalization group approach for the present system.

I. BAND STRUCTURE AS FUNCTION OF PRESSURE

The starting point for the spin-fluctuation pairing calculations is a tight binding representation of the electronic structure as a function of pressure which we obtain as follows. Starting from the lattice constants as determined experimentally in [1], we fit these with a polynomial of second order to obtain a smooth behavior of the lattice constants as a function of pressure in order to avoid non-monotonous evolution of the Fermi surface and low energy band structure. In Fig. S1, we show the experimental data together with the lattice constants as used in our *ab initio* calculations using the full-potential local-orbital (FPLO) code - version 18.00-52 [2] with the non-relativistic LSDA ("Perdew Wang 92") approximation [3]. The crystal structure of CrB_2 belongs to the space group $P6/mmm$ (# 191) and the Wyckoff positions of Cr and B atoms are $(0,0,0)$ and $(1/3,2/3,1/2)$, respectively. A $\mathbf{k}$ -grid of $12\times12\times12$ is used. Convergence is checked with respect to the $\mathbf{k}$-grid and relativistic effects are found to have negligible influence on the band structure close to the Fermi level.

For the downfolding to a tight binding model, we use the following initial projections of all five Cr $3d$ orbitals, the two B p_z orbitals and three bonding sp_2 orbitals of the two B atoms (10 orbital model). For a 13 orbital model, we additionally take into account three antibonding sp_2 orbitals. This downfolding yields a tight binding model with

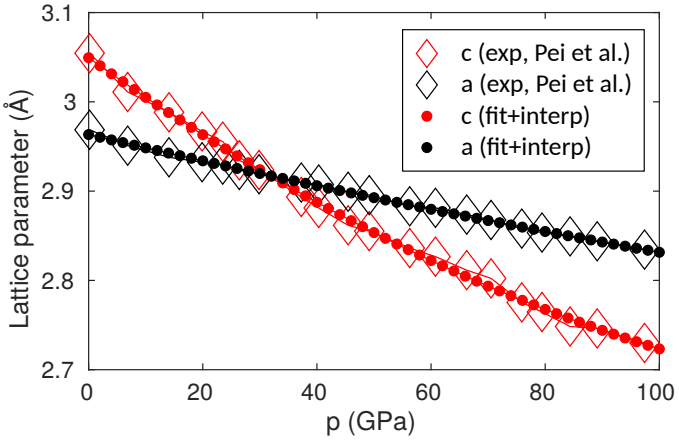

FIG. S1. Lattice parameters c and a in Å as used for the DFT calculation to obtain the tight binding model. The open diamonds are experimental data and full circles show the fit using a polynomial of second order and interpolation to obtain lattice constants at increments of 2 GPa.

* biswas@itp.uni-frankfurt.de
† kreisel@nbi.ku.dk

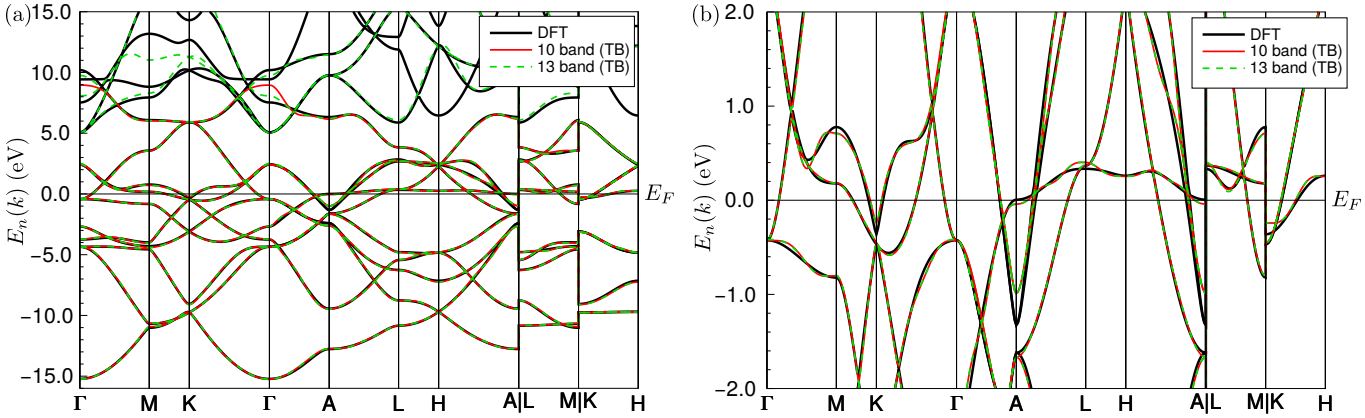

FIG. S2. Wannier downfolding. Comparison of DFT derived bands (black) with a downfolding to 10 bands (red) and downfolding to 13 bands (green, dashed) where also the antibonding orbitals are taken into account. (a) Bands at large energy scale and (b) blowup close to the Fermi level such that small deviations can be observed for few bands. (Calculation for a pressure of 25 GPa.)

roughly 20000 real-valued hoppings (for the 10 band model) up to imaginary parts of relative order 10^{-8} which are set to zero. This Hamiltonian can be written in momentum space as,

$$H_0 = \sum_{\mathbf{k}\sigma\ell\ell'} t_{\mathbf{k}}^{\ell\ell'} c_{\ell\sigma}^{\dagger}(\mathbf{k}) c_{\ell'\sigma}(\mathbf{k}), \tag{S1}$$

where $c_{\ell\sigma}^{\dagger}(\mathbf{k})$ is the Fourier amplitude of an operator $c_{i\ell\sigma}^{\dagger}$ that creates an electron in Wannier orbital ℓ with spin σ and $t_{\mathbf{k}}^{\ell\ell'}$ is the Fourier transform of the hopping elements connecting states ℓ and ℓ'. The dependence on the cutoff in distance and energy has been checked and set to `ham_cutoff 20.0` and `WF_ham_threshold 0.0001` to yield the tight binding bands as shown in Fig. S2.

II. SPIN-FLUCTUATION CALCULATIONS

The spin-fluctuation pairing calculations are based on the tight-binding formulation, as given in Eq. (S1), where we start to calculate the two-point functions, i.e. the (generalized) susceptibility in the paramagnetic state [4],

$$\chi^0_{\ell_1\ell_2\ell_3\ell_4}(q) = -\sum_{k,\mu,\nu} M^{\mu\nu}_{\ell_1\ell_2\ell_3\ell_4}(\mathbf{k},\mathbf{q}) G^{\mu}(k+q) G^{\nu}(k)\,. \tag{S2}$$

Here, we have adopted the shorthand notation $k \equiv (\mathbf{k}, \omega_n)$ for the momentum and frequency. The matrix elements are given by,

$$M^{\mu\nu}_{\ell_1\ell_2\ell_3\ell_4}(\mathbf{k},\mathbf{q}) = a_{\nu}^{\ell_4}(\mathbf{k}) a_{\nu}^{\ell_2,*}(\mathbf{k}) a_{\mu}^{\ell_1}(\mathbf{k}+\mathbf{q}) a_{\mu}^{\ell_3,*}(\mathbf{k}+\mathbf{q}), \tag{S3}$$

and the Green's function in band space reads as:

$$G^{\mu}(\mathbf{k},\omega_n) = [i\omega_n - E_{\mu}(\mathbf{k})]^{-1}. \tag{S4}$$

Next, we calculate the interacting susceptibility in a random phase approximation (RPA), where bubble diagrams are partially re-summed to get

$$\chi^{\mathrm{RPA}}_{(0,1)\,\ell_1\ell_2\ell_3\ell_4}(\mathbf{q},\omega) = \left\{ \chi^0(\mathbf{q},\omega) \left[1 - \bar{U}^{(s,c)} \chi^0(\mathbf{q},\omega) \right]^{-1} \right\}_{\ell_1\ell_2\ell_3\ell_4}. \tag{S5}$$

In this equation, $\bar{U}^{(s,c)}$ is the matrix for the generalized spin (s) and charge (c) interactions containing the parameters of the Hubbard-Kanamouri Hamiltonian, U, U', J, J', which we choose to be (spin) rotationally invariant, $U' = U - 2J$, $J = J'$ and nonzero only in the Cr $3d$ orbital components. This choice is guided by the expectation that the B orbitals are less correlated and it avoids possible complications originating from the bonding/antibonding B orbitals as these

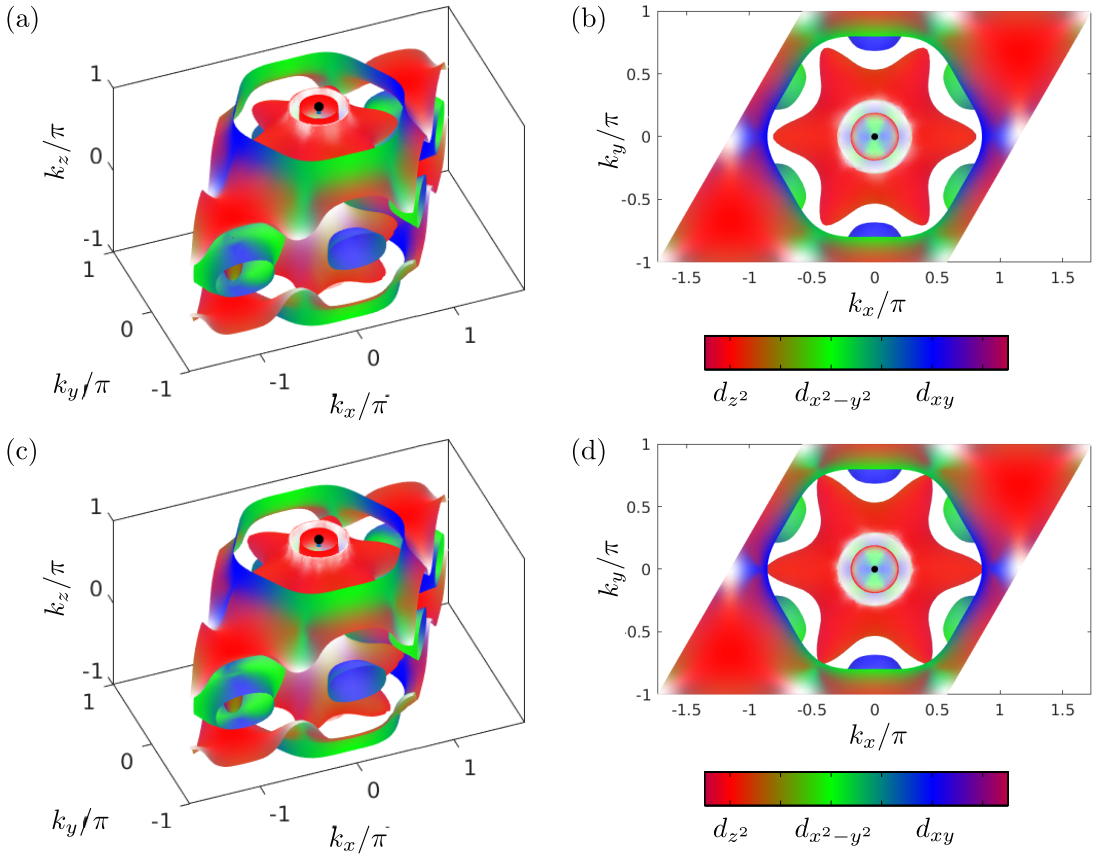

FIG. S3. Fermi surface from the 10 band model (a-b) and the 13 band model (c-d) for $p = 25\,\mathrm{GPa}$. Colors represent the different Wannier states as indicated in the legend, bright color indicates significant weight of other states.

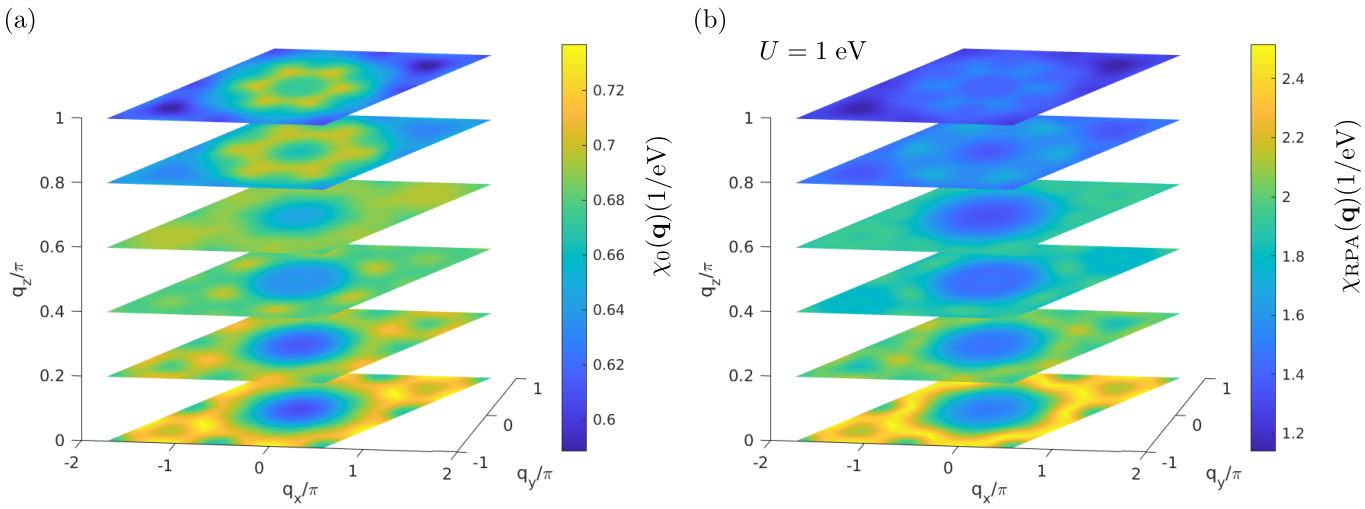

FIG. S4. Bare susceptibility calculated for $p = 24$ GPa (a) and RPA susceptibility (b) in the Brillouin-zone showing that the RPA modifies the peak structure.

are not centered at an atomic position. Moreover, a 'fully local' interaction Hamiltonian would not be an appropriate starting point. The pairing interaction in the orbital space in given by [4–6],

$$\Gamma_{\ell_1\ell_2\ell_3\ell_4}(\mathbf{k},\mathbf{k}') = \frac{1}{2}\left[3\bar{U}^s\chi_1^{\mathrm{RPA}}(\mathbf{k}-\mathbf{k}')\bar{U}^s + \bar{U}^s - \bar{U}^c\chi_0^{\mathrm{RPA}}(\mathbf{k}-\mathbf{k}')\bar{U}^c + \bar{U}^c\right]_{\ell_1\ell_2\ell_3\ell_4}, \tag{S6}$$

where χ_0^{RPA} is the charge susceptibility and χ_1^{RPA} the spin susceptibility in RPA approximation [4] at zero frequency. We deduce the leading and sub-leading superconducting instabilities from solving the linearized gap equation

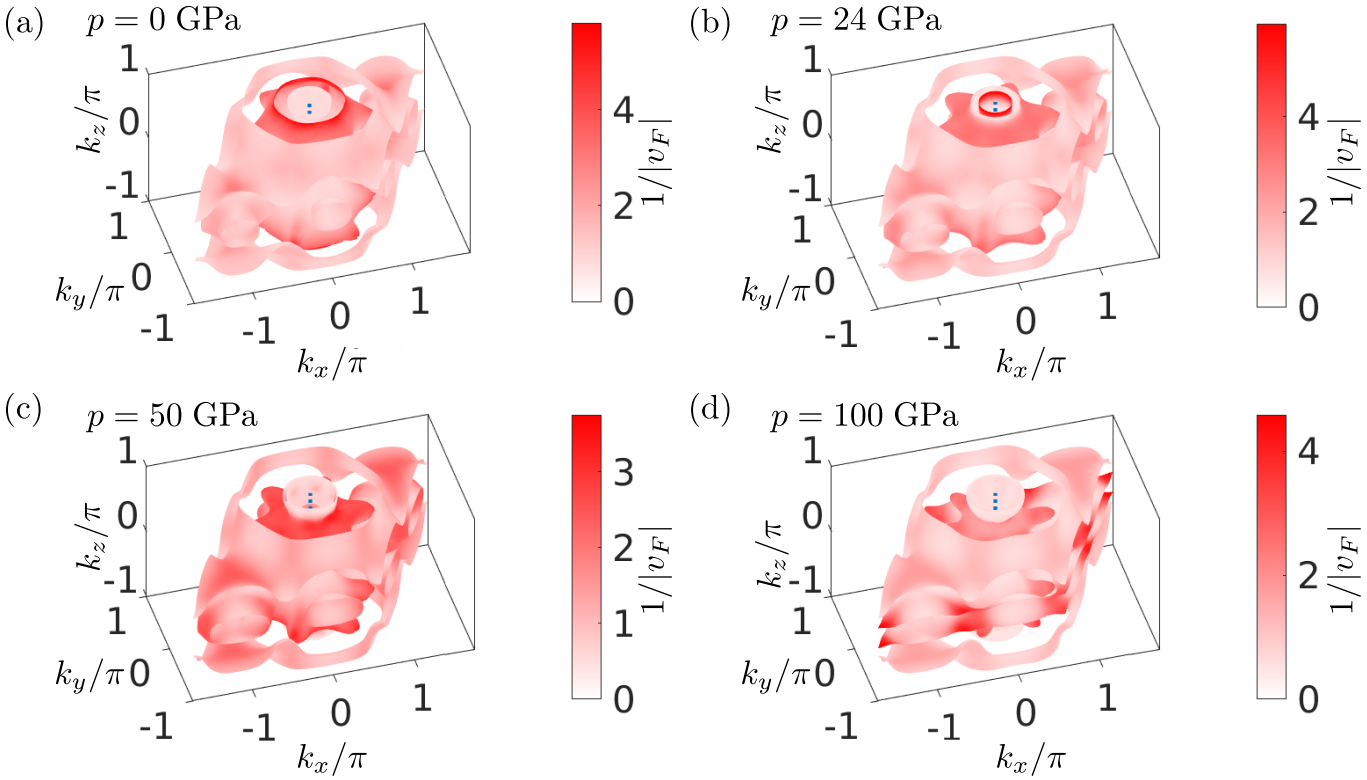

FIG. S5. Examples of Fermi surfaces with inverse Fermi velocity for pressures 0, 24, 50, 100 GPa.

(parametrized on three-dimensional Fermi surfaces [5, 6]),

$$-\frac{1}{V_G}\sum_{\mu}\int_{\mathrm{FS}_\mu} dS'\,\Gamma_{\nu\mu}(\mathbf{k},\mathbf{k}')\frac{g_i(\mathbf{k}')}{|v_{\mathrm{F}\mu}(\mathbf{k}')|} = \lambda_i g_i(\mathbf{k})\,, \tag{S7}$$

for the eigenvalues λ_i and the eigenvectors $g_i(\mathbf{k})$. The pairing interaction is projected into band space by

$$\Gamma_{\nu\mu}(\mathbf{k},\mathbf{k}') = \mathrm{Re}\sum_{\ell_1\ell_2\ell_3\ell_4} a_\nu^{\ell_1,*}(\mathbf{k})a_\nu^{\ell_4,*}(-\mathbf{k})\Gamma_{\ell_1\ell_2\ell_3\ell_4}(\mathbf{k},\mathbf{k}')\; a_\mu^{\ell_2}(\mathbf{k}')a_\mu^{\ell_3}(-\mathbf{k}')\;, \tag{S8}$$

where $a_\nu^\ell(\mathbf{k})$ is the matrix element of orbital ν for the unitary transformation to band space of band ℓ. The integral is done over the Fermi surface dS with total surface V_G and weights are given by the inverse Fermi velocity $v_{\mathrm{F}\mu}(\mathbf{k})$. The leading instability, identified by the largest eigenvalue λ_i, will lead to a superconducting order parameter $\Delta(\mathbf{k})$ that is proportional to $g_i(\mathbf{k})$ at T_c.

Tests on model dependence

The pairing calculation based on a 13 orbital model using a complex three-dimensional Fermi surface geometry is, although challenging, numerically feasible. However, for a sweep of the pressure dependence, we restricted our analysis to the 10 orbital tight binding model only and additionally constrained the calculation of the susceptibility, Eq. (S2), to the components of the 5 Cr-d orbitals. This approximation is expected to be very good given that the partial density of states of the other 5 (or 8 for the 13 orbital model) orbitals at low energies is very small and thus the respective components of the susceptibility tensor are small as well. In the pairing vertex (in our approximation), the spin and charge matrices, $\bar{U}^{(s,c)}$, only have nonzero elements for the correlated Cr-d orbitals. Therefore the only correction from the B-type orbitals are originating from the off-diagonal elements in the RPA approach, i.e. from inversion of the matrix in Eq. (S5). We checked the validity of the previous arguments by performing calculations using all components in the 10 and 13 orbital model at a selected pressure and comparing the results for the pairing eigenvalues λ_is and pairing states $g_i(\mathbf{k})$. These values come out to be very similar.

We perform the calculations for the pairing using few thousands of $\mathbf{k}$ points on the three dimensional Fermi surface and use $(105)^3$ points for the Brillouin zone integrals in the susceptibility which is typically done at a temperature

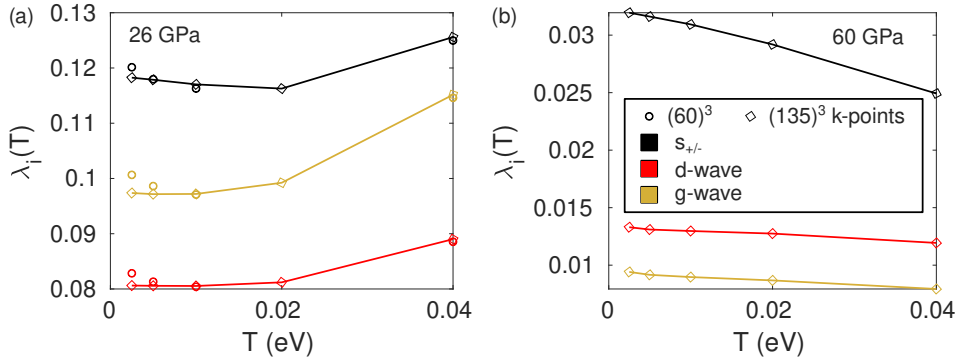

FIG. S6. Eigenvalues of the linearized gap equation at two selected pressures (a) 26 GPa and (b) 60 GPa, calculated at different temperatures. Connected data points are with high momentum resolution of $(135)^3$ k-points for the integration, while the open circles in panel (a) are for $(60)^3$ k-points revealing the expected slower convergence at low temperature.

of $T = 0.02$eV for convergence purposes that we explicitly checked. Lowering the temperature significantly increases the numerical effort to reach convergence, but does not change conclusions on the eigenvalues λ_i and leading pairing states $g_i(\mathbf{k})$ which we checked for selected pressure values, see Fig. S6. In summary, we do not expect crossings of eigenvalues of different symmetries as a function of temperature and therefore, the choice of $T = 0.02$eV is sufficient for the calculations. Very close to the magnetic instability (where the eigenvalues become much larger), the peak structure of the RPA susceptibility might sharpen up as temperature is lowered; this however is rather an artifact of the approach that ignores feedback from the imaginary part of the self energy that would broaden the peaks; an effect that is similar to the Fermi function in calculations at higher temperature.

III. ELECTRON-PHONON CALCULATIONS

All the geometric optimizations (relaxations) at fixed pressures are performed using density functional theory (DFT) as implemented in Vienna *ab initio* simulation package (vasp) [7] with plane-wave basis set (cutoff of 500 eV) and projected augmented wave (PAW) pseudopotentials. A $12 \times 12 \times 12$ Monkhorst-Pack **K**-grid is employed to perform structural relaxations until the maximum force for each component on each individual atom is smaller than 0.001 eV/Å. We find that the relaxed structures differ only on the lattice parameter c with respect to the experimental lattice parameters, see Fig. S7. This explains the reason behind finding a phonon instability of the experimental structure along the crystallographic direction c, as shown below.

We have performed *ab initio* density functional perturbation theory (DFPT) [8] calculations in order to obtain the phonon dispersions and electron-phonon coupling (EPC) constants, as implemented in Quantum ESPRESSO [9]. We used plane waves basis sets with cutoff of 80 Ry (and of 800 Ry for the corresponding charge densities) in combination with ultrasoft pseudopotentials in the generalized gradient approximations (GGA).

Using the above parameters, electron-phonon coefficients are calculated from the derivative of the self-consistent

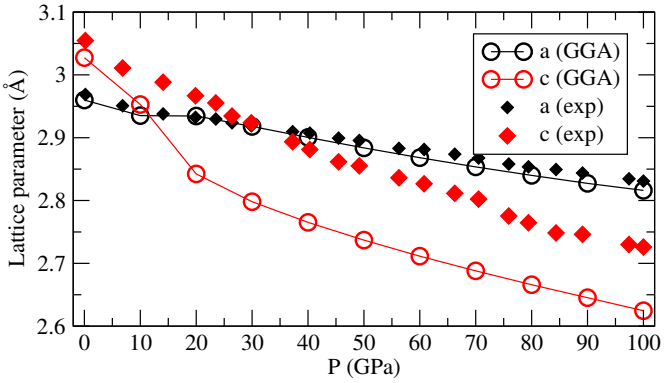

FIG. S7. Comparison of experimental and calculated lattice parameters. The calculated in-plane lattice parameters, $a = b$, compares very well with experiment. However, the calculated parameters c always remains lower than the experimental value.

Kohn-Sham potentials, $V_{\rm SCF}$, using

$$g_{mn,\nu}(\mathbf{k},\mathbf{q}) = \frac{1}{\sqrt{2\omega_{q,\nu}}}\langle\Psi_{m,\mathbf{k+q}}|\partial_{\mathbf{q},\nu}V_{\rm SCF}|\Psi_{n,\mathbf{k}}\rangle, \tag{S9}$$

where m, n are the band indices and $\mathbf{k}, \mathbf{q}$ are the electron and phonon wavevectors.

The electron-phonon line-width and the spectral function α^2F are then calculated using the following equations:

$$\gamma_{\mathbf{q},\nu} = 2\pi\omega_{\mathbf{q},\nu}\sum_{m,n}\int\frac{d^3k}{\Omega_{BZ}}|g_{mn,\nu}(\mathbf{k},\mathbf{q})|^2\delta(\epsilon_{m,\mathbf{k+q}}-\epsilon_F)\delta(\epsilon_{n,\mathbf{k}}-\epsilon_F)\text{and} \tag{S10}$$

$$\alpha^2F(\omega) = \frac{1}{2\pi N_F}\sum_{\mathbf{q},\nu}\delta(\omega-\omega_{\mathbf{q},\nu})\frac{\gamma_{\mathbf{q},\nu}}{\hbar\omega_{\mathbf{q},\nu}}. \tag{S11}$$

EPC constants are then calculated by,

$$\lambda = 2\int_0^{\omega_{\rm max}}\alpha^2F(\omega)d\omega, \tag{S12}$$

where $\omega_{\rm max}$ is the maximum phonon frequency at a given pressure. The superconducting T_c has been calculated by employing the McMillan-Allen-Dynes formula [10, 11]:

$$T_c = \frac{\omega_{\log}}{1.2}\exp\left(\frac{-1.04(1+\lambda)}{\lambda-\mu_c^*(1+0.62\lambda)}\right), \tag{S13}$$

where $\omega_{\log}$ is the logarithmic average of the phonon frequency in the Eliashberg theory and μ_c^* is the effective Coulomb parameter which has been taken to be 0.1.

As mentioned in the main text and shown in Fig. S8, the phonon dispersions show imaginary frequencies over the entire pressure range (only two pressure values are taken for demonstration) when we keep the structures at the experimental lattice constants [1]. As the calculation of electron-phonon coupling generally requires a very good convergence check of **k**-mesh and **q**-meshes, we had performed the convergence tests for the relaxed (calculated) structure at 100 GPa as shown in Figs S9 and S10. We take the converged values of **k**-mesh **q**-mesh to be $30\times30\times30$ and $10\times10\times10$, respectively and Gaussian smearing value is 0.004 Ry.

We have, however, estimated the values of EPC constants, λ, and critical temperature, T_c, in experimental structures at 60.77 and 100 GPa by removing the imaginary frequencies which give the lower bound of λ. We found the values of T_c are 14.3 K at 100 GPa and 13.6 K at 60.77 GPa, giving rise to a slope of 0.018 in the pressure-temperature plot. This is motivated us to draw the 'EPC-only' contribution (black line) as linear in Fig. 1 of the main text. Note that for the relaxed structure at 100 GPa where all phonon modes are stable, the value of T_c is 17 K. These values of T_cs are obtained by using McMillan-Allen-Dynes formula [10, 11]. It is evident that there is only a small difference in calculated T_c at 100 GPa for the experimental and relaxed structures and both these values are considerably higher than the experimental T_c of 7 K. This hints at the suppression of effective T_c by pair-breaking spin-fluctuations as mentioned in the main text.

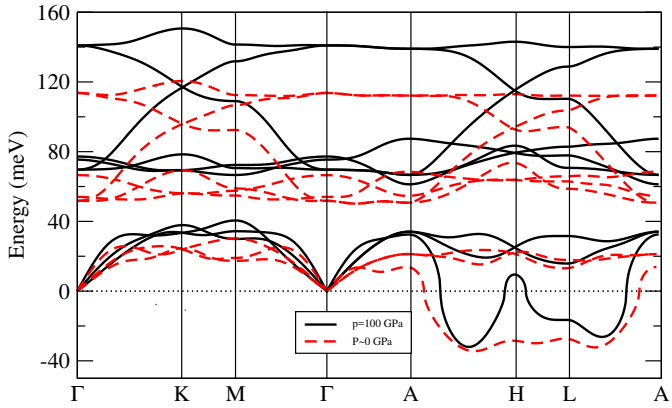

FIG. S8. Phonon dispersion at ambient (red dashed lines) and 100 GPa (black solid lines) pressure with structures at experimental lattice constants.

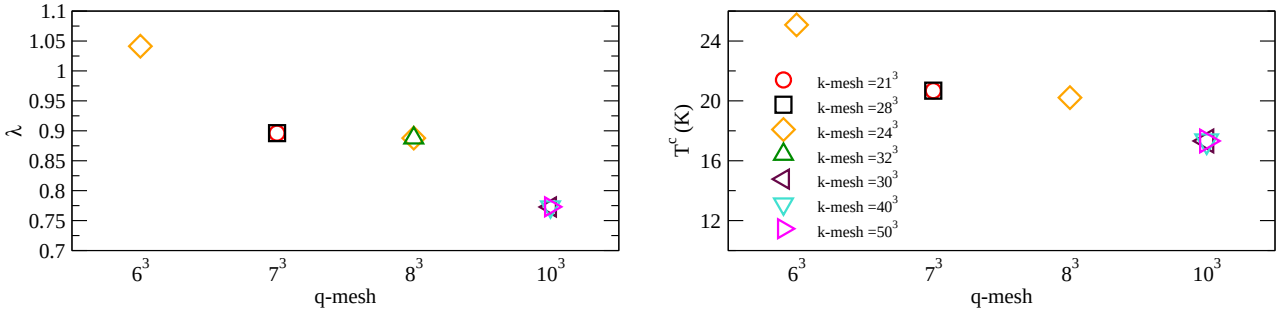

FIG. S9. Convergence tests for electron-phonon coupling constant, λ and T_c with fixed Gaussian broadening 0.005 (Ry) for different **k**-mesh and **q**-mesh.

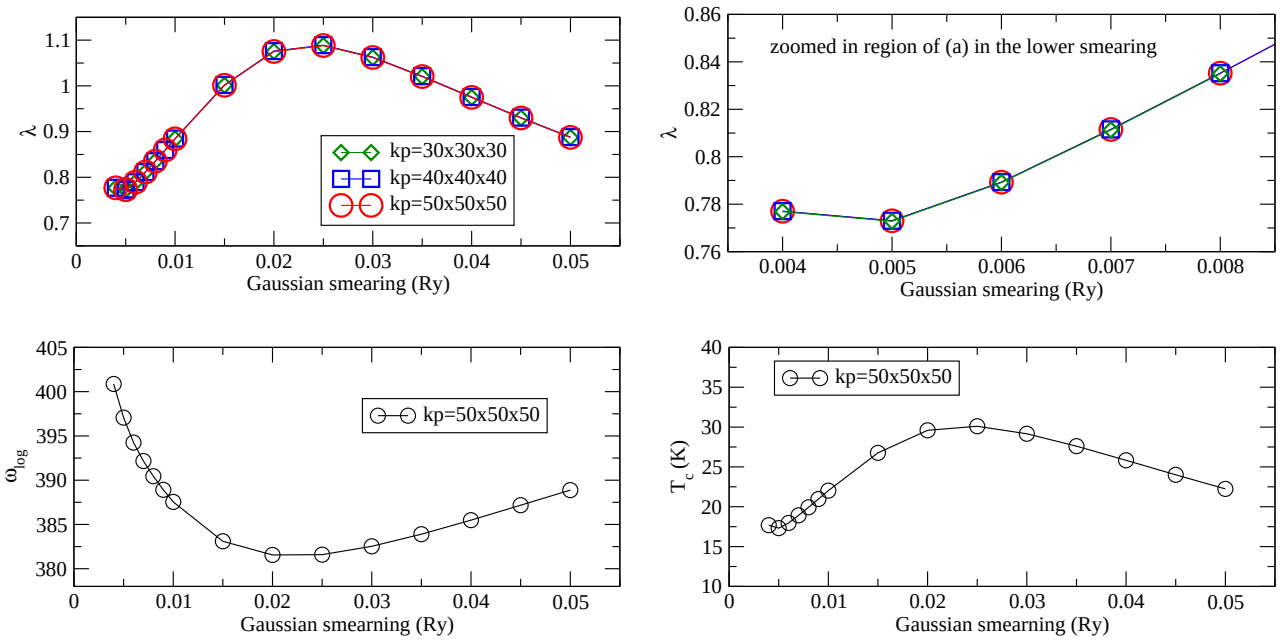

FIG. S10. Convergence tests for electron-phonon coupling constant, λ, ω_{log} and T_c with Gaussian smearing value and **k**-mesh, for fixed **q**-mesh=$10 \times 10 \times 10$.

IV. CHARGE DENSITY WAVE (CDW) STATES

Phonon dispersions of the experimental structures [1] show dynamic instabilities through the appearance of an imaginary longitudinal acoustic mode along the c-direction which is plotted as negative frequencies in Fig. S8. Note that these instabilities appear at all pressures for the experimental structures. Below we show that CrB_2 under pressure develops a charge density wave (CDW) state.

We have performed a supercell calculation at 100 GPa following the phonons instability perpendicular to the hexagonal boron plane. Relaxation of the supercell ($\sqrt{3}a \times 3a \times 2c$) gives rise to a body-centered orthorhombic structure, where one third of the Cr atom is puckered (by 0.085 Å) along the c-direction due to application of pressure, in addition to the appearance of nonuniform Cr bonds (which differ by maximum amount of 0.024 Å). The conventional cell is 4.5 meV/CrB_2 higher in energy than the supercell, suggesting a CDW state with $q = 1/3, 1/2, 1/2$. However, zero-point vibrational fluctuations may stabilize the conventional structure.

V. TWO BAND TOY MODEL

To illustrate the effect of pair breaking from spin-fluctuation pairing processes in combination with electron-phonon pairing, we consider a simple two band toy model and cast the linearized gap equation, Eq. (S7) into a 2×2 matrix

equation

$$-\underline{V}\, g_\pm = \lambda_\pm g_\pm \tag{S14}$$

where $\underline{V} = (\underline{V^{\rm SF}} + \underline{V^{\text{el-ph}}})\,\underline{\rho}$ is the (averaged over the Fermi surface) pairing interaction from spin- fluctuations (SF) and from the electron-phonon (el-ph) mechanism and $\underline{\rho}$ is a (diagonal) matrix with the partial densities of states of the two bands. $\lambda_\pm$ are the two eigenvalues to the two eigenvectors $g_\pm$. For simplicity, we assume two bands with identical density of states, $\underline{\rho} = \rho_0\delta_{ij}$ and parametrize the pairing interactions (including the density of states prefactor as follows). The electron-phonon pairing in CrB_2 is dominated by small momentum transfer $\mathbf{q}$, thus we assume it to be intra-band only,

$$\underline{V^{\text{el-ph}}}\,\underline{\rho} = \begin{pmatrix} \alpha & \epsilon \\ \epsilon & \alpha \end{pmatrix}\,, \tag{S15}$$

i.e. $|\alpha| \gg |\epsilon|$. The spin-fluctuation part has intra-band and inter-band contributions,

$$\underline{V^{\rm SF}}\,\underline{\rho} = \begin{pmatrix} \beta & \delta \\ \delta & \beta \end{pmatrix}\,. \tag{S16}$$

The spin-fluctuation pairing has the following dependence on the susceptibility $\Gamma \sim U + U^2\chi(\mathbf{q})^{\rm RPA} = U + U^2\chi(\mathbf{q})^0/(1 - U\chi(\mathbf{q})^0)$ where $\mathbf{q}$ is either the sum or difference of the scattering vectors connecting the two Fermi surfaces (when projecting the pairing interaction into the singlet channel). With the expected behavior of the susceptibility close to a nesting condition of $\chi^0(\mathbf{q}) = \gamma/(1 + (\mathbf{q} - \mathbf{q}_c)^2\xi^2)$ where $\mathbf{q}_c$ is the nesting vector, ξ the correlation length of the spin-fluctuations and γ proportional to the (inverse) bandwidth W of the electronic structure. We are assuming further the following linear dependence of the bandwidth $W(p) = W_{\rm AFM}(1 + x(p - p_c))$, where $W_{\rm AFM}$ is the bandwidth at the antiferromagnetic instability, p_c is the corresponding critical pressure and x the coefficient from the Taylor expansion. In rewriting the pairing problem into a 2x2 matrix problem, we assume that the pairing can be simplified into interband pairing and intraband pairing contributions that are dominated by the susceptibility at a fixed momentum transfer $\mathbf{q}$, such that the matrix elements can be written as

$$\beta = \Gamma(\mathbf{q})\rho_0 \sim \Big(U + \frac{U^2\frac{A_1}{W(p)}}{1 - U\frac{A_1}{W(p)}}\Big)\frac{g}{W(p)}\,, \tag{S17}$$

where we have used that also the density of states scales with the bandwidth $\rho_0 = g/W(p)$ and the parameter A_1 is the ratio between the (bare) susceptibility at the momentum transfer $\mathbf{q}$ and the bandwidth, $A_1 = \chi^0(\mathbf{q})/W(p)$. Rewriting the fraction and setting $\beta_0 = Ug/W_{\rm AFM}$ and $\alpha_1 = UA_1/W_{\rm AFM}$ we arrive at the coefficient $\beta = \beta_0/(1 - \alpha_1 + x(p - p_c))$ parametrized as function of the pressure p. A similar expression is given for the intraband pairing contribution $\delta = \beta_0/(1 - \alpha_2 + x(p - p_c))$. The parameters α_i control the closeness to the nesting condition, i.e. $\alpha_i = 1$ is perfect nesting of all k-points on the Fermi surfaces and $\alpha_i = 0$ no nesting such that the susceptibility is just given by the background from the density of states at the Fermi level. Note that this simple parametrization correctly captures the leading behavior of the pairing interaction as approaching $p \to p_c$ (where the constant part U can be neglected) and the behavior at large bandwidth where the matrix of the spin fluctuation pairing has elements with almost identical values. Looking at the two parts of the pairing interaction separately, it is evident that the matrix in Eq. (S15) yields two positive eigenvalues with eigenvectors $g_+ = (1, 1)/\sqrt{2}$ and $g_- = (1, -1)/\sqrt{2}$ where the first has larger eigenvalue and corresponds to the (usual) s_{++} pairing state. The matrix in Eq. (S16) has the same eigenvectors, where only g_- yields a positive eigenvalue. In Fig. S11 we show the overall behavior of the individual eigenvalues and the combined pairing interaction that leads to a significantly reduced eigenvalue and thus T_c close to the antiferromagnetic instability and a change of the pairing state from $s_\pm$ to s_{++} as pressure increases. Note that our RPA approach for pairing does not take into account retardation effects. In the real system, the onsite U, being a high-energy interaction, will be renormalized and logarithmically suppressed, which is usually expressed in terms of μ_c^*.

VI. FUNCTIONAL RENORMALIZATION GROUP (FRG) CALCULATIONS

The inherent three dimensionality and the importance of multi-orbital features in CrB_2 present significant challenges for any many body calculation in this system. While these conditions pose a significant challenge for our RPA analysis, they become insurmountable for functional renormalization group (fRG) calculations. Since the fRG extends the analysis of the effective interaction beyond the Cooper channel, an at least approximate treatment of the full momentum dependence for the two-particle vertex function is a prerequisite. In the most modern formulation of the fRG, the truncated unity (TU) approximation, an RPA result guided resolution would still necessitate an effective

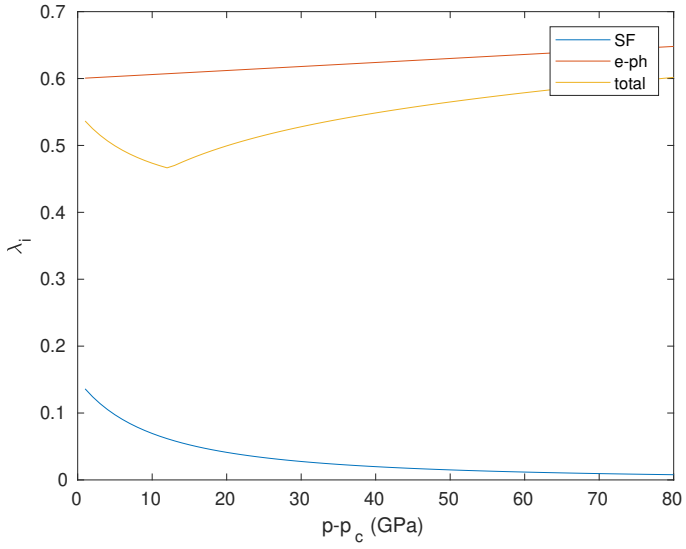

FIG. S11. Cooperation and competition of spin-fluctuation pairing and electron-phonon pairing. Plot of the largest eigenvalues for the two band model showing the transition from an $s_{\pm}$ state with sizable spin-fluctuation pairing close to the antiferromagnetic instability at p_c to an ordinary s_{++} state where pair-breaking effects from spin-fluctuations are still sizeable.

vertex description with over 20 billion parameters. Within the fRG this equates to the solution of a coupled system of 20 billion integro-differential equations which is far beyond the current cutting edge of possibilities. The problem is further complicated by the TU-approximations incompatibility with the use of a natural basis for an efficient implementation of symmetries [12].

[1] C. Pei, P. Yang, C. Gong, Q. Wang, Y. Zhao, L. Gao, K. Chen, Q. Yin, S. Tian et al., Pressure-induced superconductivity in itinerant antiferromagnet CrB_2, arXiv:2109.15213 10.48550/ARXIV.2109.15213 (2021).

[2] K. Koepernik and H. Eschrig, Full-potential nonorthogonal local-orbital minimum-basis band-structure scheme, Phys. Rev. B **59**, 1743 (1999).

[3] J. P. Perdew and Y. Wang, Accurate and simple analytic representation of the electron-gas correlation energy, Phys. Rev. B **45**, 13244 (1992).

[4] S. Graser, T. A. Maier, P. J. Hirschfeld and D. J. Scalapino, Near-degeneracy of several pairing channels in multiorbital models for the Fe pnictides, New Journal of Physics **11**, 025016 (2009).

[5] A. Kreisel, Y. Wang, T. A. Maier, P. J. Hirschfeld and D. J. Scalapino, Spin fluctuations and superconductivity in $K_xFe_{2-y}Se_2$, Phys. Rev. B **88**, 094522 (2013).

[6] M. Dürrnagel, J. Beyer, R. Thomale and T. Schwemmer, Unconventional superconductivity from weak coupling, The European Physical Journal B **95**, 112 (2022).

[7] G. Kresse and J. Hafner, Ab initio molecular dynamics for liquid metals, Phys. Rev. B **47**, 558 (1993).

[8] S. Baroni, S. de Gironcoli, A. Dal Corso and P. Giannozzi, Phonons and related crystal properties from density-functional perturbation theory, Rev. Mod. Phys. **73**, 515 (2001).

[9] P. Giannozzi, S. Baroni, N. Bonini, M. Calandra, R. Car, C. Cavazzoni, D. Ceresoli, G. L. Chiarotti, M. Cococcioni et al., QUANTUM ESPRESSO: a modular and open-source software project for quantum simulations of materials, Journal of Physics: Condensed Matter **21**, 395502 (2009).

[10] W. L. McMillan, Transition temperature of strong-coupled superconductors, Phys. Rev. **167**, 331 (1968).

[11] P. B. Allen and R. C. Dynes, Transition temperature of strong-coupled superconductors reanalyzed, Phys. Rev. B **12**, 905 (1975).

[12] J. Beyer, J. B. Hauck and L. Klebl, Reference results for the momentum space functional renormalization group, The European Physical Journal B **95**, 65 (2022).